

Using R2* values to evaluate brain tumours on magnetic resonance imaging: Preliminary results

Zhenghua Liu · Haibo Liao · Jianhua Yin · Yanfang Li

Received: 20 May 2013 / Revised: 8 October 2013 / Accepted: 10 October 2013 / Published online: 26 November 2013
© European Society of Radiology 2013

Abstract

Objective To determine the usefulness of the R2* value in assessing the histopathological grade of glioma at magnetic resonance imaging and differentiating various brain tumours. **Methods** Sixty-four patients with brain tumours underwent R2* mapping and diffusion-weighted imaging examinations. ANOVA was performed to analyse R2* values among four groups of glioma and among high-grade gliomas (grades III and IV), low-grade gliomas (grades I and II), meningiomas, and brain metastasis. Spearman's correlation coefficients were used to determine the relationships between the R2* values or apparent diffusion coefficient (ADC) and the histopathological grade of gliomas. R2* values of low- and high-grade gliomas were analysed with the receiver-operator characteristic curve.

Results R2* values were significantly different among high-grade gliomas, low-grade gliomas, meningiomas, and brain metastasis, but not between grade I and grade II or between grade III and grade IV. The R2* value (18.73) of high-grade gliomas provided a very high sensitivity and specificity for differentiating low-grade gliomas. A strong correlation existed between the R2* value and the pathological grade of gliomas.

Conclusions R2* mapping is a useful sequence for determining grade of gliomas and in distinguishing benign from malignant tumours. R2* values are better than ADC for characterising gliomas.

Key Points

- Magnetic resonance imaging parameters are increasingly used to assess cerebral lesions.
- R2* values are better than diffusion weighting for characterising gliomas.
- R2* values can help distinguish among different grades of glioma.
- Significant difference existed in R2* values between high- and low-grade gliomas.

Keywords R2* values · Glioma · ASL · DWI · Metastasis

Introduction

Meningioma, brain metastasis, and glioma are the three most common types of brain tumours [1, 2]. According to the 2007 World Health Organisation (WHO) grading system, tumours of glial origin are typically classified into four grades (I, II, III, and IV) [3]. Accurate preoperative diagnosis is very important in patients with brain tumours because treatment approaches depend on the histopathological type and grade of the tumours [4–6].

Advanced MRI techniques such as arterial spin labelling (ASL) perfusion imaging and diffusion-weighted imaging (DWI) can greatly improve the diagnostic accuracy in cancer [7–10]. ASL can measure regional cerebral blood flow (rCBF), which is closely correlated with tumour grade [11].

The T2* mapping sequence is an advanced MRI technique that reflects changes in the deoxygenated haemoglobin concentration of human tissue [12]. Because oxygenated haemoglobin is diamagnetic and deoxygenated haemoglobin is paramagnetic, an increase in deoxygenated haemoglobin concentration can lead to an increase in magnetic field heterogeneity, which can result in a decrease in signal intensity on T2*-weighted images, with resultant shortening of T2*

Z. Liu (✉) · H. Liao · J. Yin
The Department of Magnetic Resonance Imaging, Medical Image Center, the Second Affiliated Hospital of Nanchang University, 1, Minde Road, Donghu District, Nanchang, China 330006
e-mail: wuxiaoshui@126.com

Y. Li
The Department of Preventive Medicine, Heze Medical College, 1950 University Road, HeZe, Shandong 274000, China

relaxation times [13, 14]. As a result, without administration of contrast agent, $R2^*$ ($R2^*=1/T2^*$) values can reflect the oxygenation state of tumours [15, 16]. Furthermore, the $R2^*$ value is a comparatively objective method because it is quantitative. The $R2^*$ value has been used to investigate the response of tumours when subjects breathe various gases and to predict treatment outcomes of tumours [17–21]. Some authors have found that high-grade (III–IV) gliomas have significantly lower $T2'$ values than low-grade (II) gliomas [22]. However, $T2'$ values require acquisition of $T2^*$ and $T2$ values. Therefore, the $T2'$ mapping sequence is more time-consuming than the $T2^*$ mapping sequence. In addition, the $T2'$ mapping sequence is difficult to obtain. To our knowledge, there have been no reports on the use of $R2^*$ values to evaluate brain tumours in humans. Therefore, the purpose of the study was to determine the usefulness of $R2^*$ values in assessing the histopathological grade of gliomas and differentiating between benign and malignant tumours.

Materials and methods

Study group

After obtaining local ethics committee approval, 71 patients with brain tumours were enrolled in this prospective study. All patients or their guardians signed informed consent. Seven patients were excluded because of susceptibility artefacts. Therefore, 64 patients (24 female and 40 male patients; age range, 8–75 years) took part in the study.

Inclusion criteria were as follows: (1) All MRI examinations were performed before surgical resection, chemotherapy, or radiotherapy. (2) There were no susceptibility artefacts on tumour $T2^*$ maps. (3) Brain surgery was performed in patients with glioma or meningioma confirmed by pathology. (4) The primary lesion was lung cancer in all patients with metastatic lesions in the brain and was verified by pathology after pulmonary surgery or biopsy. Six patients with solitary brain metastasis underwent brain surgery, whereas seven patients with brain metastasis who did not undergo brain surgery were followed up for 1 year. Diagnosis of brain metastasis in these seven patients was based on a history of lung cancer, brain MRI examination, and clinical follow-up.

The histopathological diagnosis in the 38 patients with gliomas yielded 5 cases of grade I, 17 cases of grade II, 7 cases of grade III, and 9 cases of grade IV. Meningioma was diagnosed in 13 patients and brain metastasis in 13 patients. The demographical data and histopathological diagnosis are listed in Table 1. Figures 1, 2 and 3 show exemplary images of gliomas with grades from II to IV, respectively. Figures 4 and 5

Table 1 Patients age and sex, pathologic diagnosis, tumour grade, and $R2^*$ and relative cerebral blood flow (rCBF) measurements

Patient No./age /sex	Pathological diagnosis	Tumour grade	$R2^*$	rCBF	ADC ($\times 10^{-3}$)
1/18/M	Astrocytoma	I (low)	11.03		1.88
2/40/F	Astrocytoma	I (low)	11.8	0.89	1.05
3/49/M	Astrocytoma	I (low)	13.88		1.26
4/17/M	SGCA	I (low)	18.34	1.38	0.87
5/9/M	SGCA	I (low)	15.05	0.73	1.08
6/47/F	Astrocytoma	II (low)	5.70	0.44	1.56
7/8/F	Astrocytoma	II (low)	18.67	0.62	0.89
8/42/F	Astrocytoma	II (low)	9.27		0.987
9/41/M	Astrocytoma	II (low)	14.25	0.85	0.773
10/35/F	Astrocytoma	II (low)	14.33	0.56	1.22
11/38/M	Astrocytoma	II (low)	15.65	1.03	
12/30/M	Astrocytoma	II (low)	12.21		1.03
13/29/F	PXA	II (low)	21.63		1.09
14/24/M	Astrocytoma	II (low)	10.80		1.06
15/48/M	Astrocytoma	II (low)	10.77	0.98	1.28
16/62/M	Astrocytoma	II (low)	14.10	0.61	1.04
17/25/F	Astrocytoma	II (low)	5.20	0.69	1.40
18/45/F	Astrocytoma	II (low)	13.65	1.04	0.694
19/28/M	Astrocytoma	II (low)	13.58	1.67	0.895
20/13/M	Ependymoma	II (low)	15.92	0.72	1.86
21/26/M	Ependymoma	II (low)	18.73	1.49	0.711
22/38/F	Astrocytoma	II (low)	9.67	0.69	1.37
23/51/F	AA	III (high)	20.44	1.03	1.15
24/9/M	AE	III (high)	29.63	1.47	0.709
25/28/M	AO	III (high)	31	1.64	0.921
26/35/F	AA	III (high)	36.95	1.65	1.16
27/37/M	AA	III (high)	25.48	2.4	1.16
28/33/F	AA	III (high)	22.28		0.939
29/30/M	AA	III (high)	18.91		0.898
30/59/F	GBM	IV (high)	29.10	1.94	0.793
31/66/M	GBM	IV (high)	28.86	0.95	0.903
32/51/M	GBM	IV (high)	34.36		1.06
33/62/M	GBM	IV (high)	36.08	1.92	0.932
34/15/F	GBM	IV (high)	36.65		0.899
	Ependymoblastoma				
35/70/M	GBM	IV (high)	28.26		1.16
36/46/M	GBM	IV (high)	32.08	1.64	0.993
37/55/M	GBM	IV (high)	23.76	1.38	0.819
38/62/M	GBM	IV (high)	29.71	3.42	0.914
39/54/F	Meningioma		23.57		
40/61/F	Meningioma		19.03		
41/57/F	Meningioma		14.49		
42/55/F	Meningioma		14.67	0.69	
43/47/F	Meningioma		16.27	0.93	
44/55/M	Meningioma		15.27		
45/27/F	Meningioma		13.64	2.83	
46/48/F	Meningioma		16.00	1.08	

Table 1 (continued)

Patient No./age /sex	Pathological diagnosis	Tumour grade	R2*	rrCBF	ADC ($\times 10^{-3}$)
47/49/M	Meningioma		22.75	5.4	
48/52/F	Meningioma		16.41	2.66	
49/61/M	Meningioma		15.58	3.00	
50/61/M	Meningioma		14.58	5.41	
51/40/M	Meningioma		20.67		
52/57/M	Metastasis, lung (no surgery)		17.81	1.01	
53/62/M	Metastasis, lung		23.59		
54/ 66/M	Metastasis, lung		19.61		
55/ 74/M	Metastasis, lung (No surgery)		25.89		
56/58/F	Metastasis, lung (no surgery)		19.50		
57/75 /M	Metastasis, lung (no surgery)		23.56		
58/ 61/M	Metastasis, lung		24.50		
59/47/M	Metastasis, lung		14.89		
60/56/M	Metastasis, lung		34.17		
61/66/M	Metastasis, lung (no surgery)		27.65	1.09	
62/70/M	Metastasis, lung (no surgery)		18.91	1.57	
63/64/M	Metastasis, lung		18.42	2.69	
64/57/F	Metastasis, lung (no surgery)		23.94	1.19	

M, male; F, female; SGCA subependymal giant-cell astrocytoma; PXA pleomorphic xanthoastrocytoma; AE anaplastic ependymoma; AO anaplastic oligodendroglioma; AA anaplastic astrocytoma; GBM, glioblastoma multiforme; rrCBF, ratio of rCBF of tumours to the contralateral normal regions

show examples of brain metastasis and meningioma, respectively. Because ASL software was not available at the beginning of the study, ASL was acquired in 40

cases: 27 cases of gliomas, 18 cases of meningiomas, and 5 cases of brain metastasis.

Imaging protocol

All MR examinations were performed at 3.0 T (Signa Excite HDxt, GE Healthcare, USA) with an eight-channel phased-array head coil. Vacuum cushions were packed into the coil to hold the patient’s head still.

The MR imaging protocol included axial T2 FLAIR, T1 FLAIR, DWI, T2* mapping, 3DASL, and contrast-enhanced (CE) T1WI. The dose of Magnevist (Gd-DTPA; Guangzhou, China) was 0.1 mmol/kg. With T2 FLAIR sequences, parameters were as follows: repetition time (TR) 3,400 ms; echo time (TE) 109 ms; time to inversion (TI) 41.7 ms, slice thickness 5 mm and a 1.5-mm gap between slices; field of view (FOV) 24×24 cm²; matrix size 320×256; number of excitations (NEX) 2. T1 FLAIR parameters were TR/TE 2,376/24 ms; TI 860 ms; slice thickness 5.0 mm; section gap 1.5 mm; FOV 24×24 cm²; matrix size 384×256; NEX 1. An axial single-shot spin-echo echo planar sequence was used to acquire DW imaging with the following parameters: TR/TE 5,600/70; b factors, 0 and 1, 000 s/mm²; matrix size, 160×160; FOV, 24×24 cm²; NEX, 4; slice thickness, 5 mm; section gap, 1.5 mm. Automatic high order B0 shimming was performed before the T2* sequence. T2* mapping parameters were TR/TE 150/2.1, 5.5, 8.9, 12.3, 15.7, 19.1, 22.4, 25.8, 29.2, 32.6, 36, and 39.4 ms; slice thickness 5.0 mm; section gap 1.5 mm; FOV 24×24 cm²; matrix size 192×160; NEX 1. 3DASL parameters were TR/TE 4,521/9.8 ms; TI 1525 ms; slice thickness 4.0 mm; section gap 0.0 mm; FOV 24×24 cm²; points 512; arms 8; NEX 3. CE-T1FLAIR parameters were TR/TE 2,071/26 ms; TI 860 ms; slice thickness 5.0 mm; section gap 1.5 mm; FOV 24×24 cm²; matrix size 320×256; NEX 2.

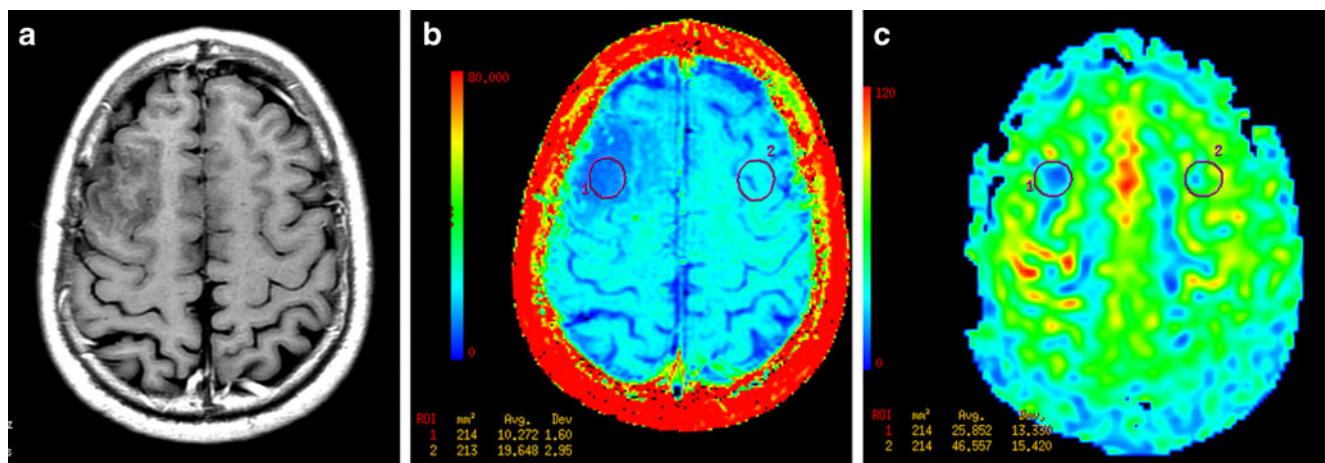


Fig. 1 Right frontal lobe astrocytoma, grade II, in a 48-year-old man. (a) Transverse contrast-enhanced T1-weighted image shows no enhancement in the tumour. (b) The R2* map shows that the R2* values in the tumour (R2* value=10.27) are lower than those in the contralateral brain

(R2* value=19.65). (c) Arterial spin labelling (ASL) regional cerebral blood flow (rCBF) map demonstrates that the tumour has low perfusion levels

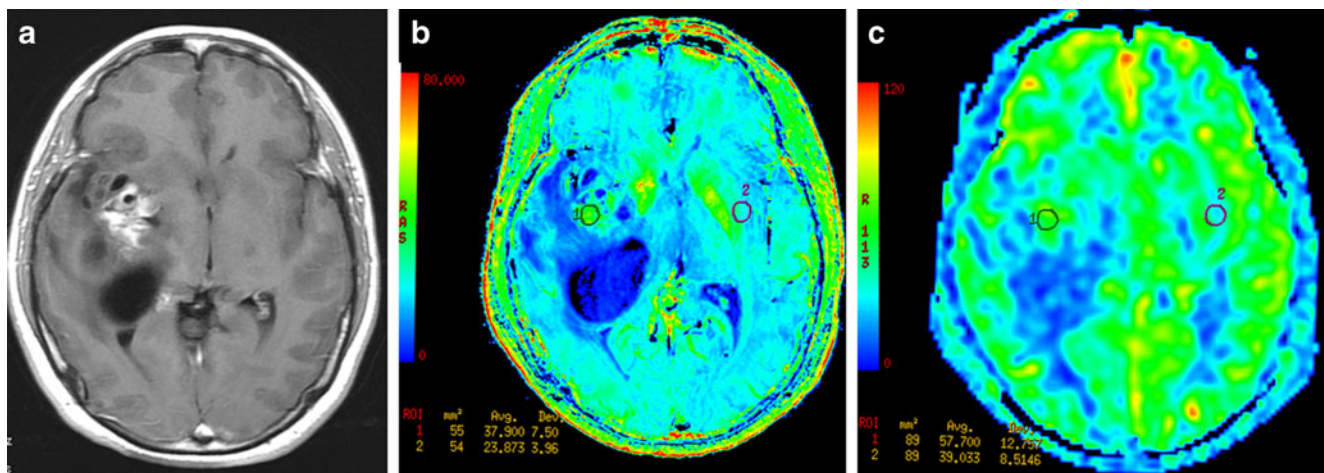


Fig. 2 Images obtained in a 35-year-old woman with anaplastic astrocytoma (grade III). (a) Transverse contrast-enhanced T1-weighted image shows heterogeneous enhancement in the tumour. (b) The R2* map

reveals that the R2* value in the tumour (R2* value=37.90) is higher than that in the contralateral brain (R2* value=23.87). (c) The ASL CBF map shows high tumour blood flow

Data processing

R2* maps were independently evaluated by two neuroradiologists (13 years of experience and 8 years of experience), who were blinded to histopathological results. The interval between the two measurements was about 2 months. ASL and DWI images were assessed by one neuroradiologist (13 years of experience). R2* maps, DWI, and ASL images were automatically reconstructed from the raw data by using the commercially available software (GE Healthcare) on an AW4.4 workstation (GE Healthcare, USA). R2*, apparent diffusion coefficient (ADC), and rCBF maps were displayed with a colour scale. T2* values were calculated based on the following formula: $SI(t) = SI_0 e^{-t/T2^*}$, where t is the echo time, $SI(t)$ is the image intensity when $t=0$, and SI_0 is the image intensity

when t =echo time. The exponential equation was fitted with nonlinear least-squares (Levenberg-Marquardt) curve fitting.

The signal-to-noise ratio (SNR) was measured for each T2* mapping image using the following formula: mean signal intensity of brain tissue/standard deviation of background noise measured outside the brain. A region of interest (ROI) with an area of 300 mm² was placed on a constant point in the unaffected frontal white matter, and another ROI of the same size was placed in the background. We set 100 as the image SNR threshold. Because SNR decreases with longer echo times, we focused on the images of the last four echoes. If the image SNR was less than 100, we rejected the images and used the former eight echoes to calculate the exponential equation. If not, we used all 12 echoes in the calculation. In the measurement, the SNR of all the images of the last four

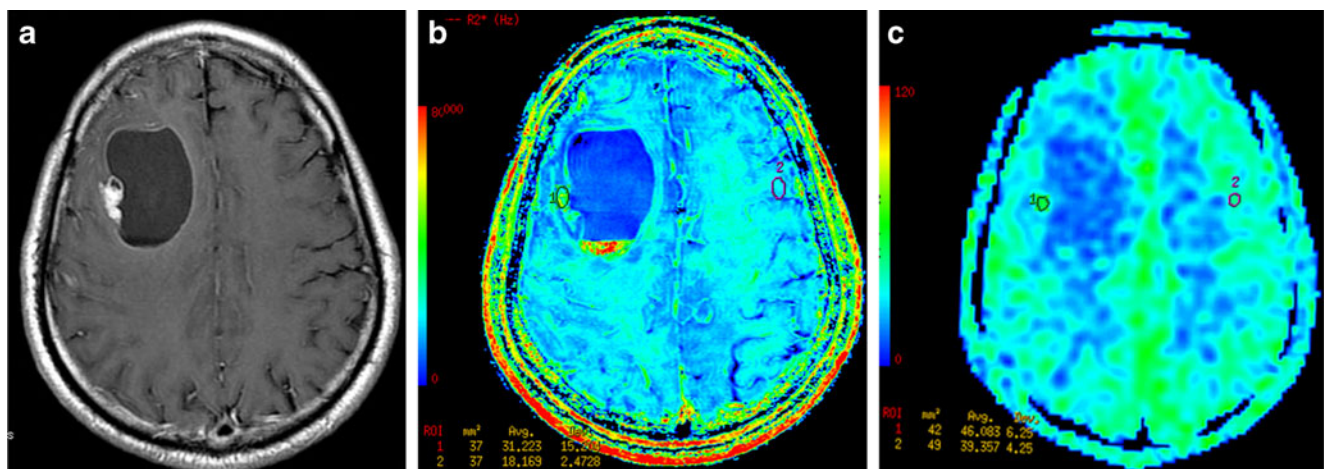


Fig. 3 A 46-year-old man with a histologically proven glioblastoma multiforme (grade IV) located in the right frontal lobe. (a) Axial T1-weighted postcontrast image demonstrates nodular enhancement in the

tumour. (b) The R2* map shows an area of high R2* values (31.22) in the tumour. There is haemorrhage at the bottom of the tumour. (c) The ASL CBF map demonstrates nodular hyperperfusion

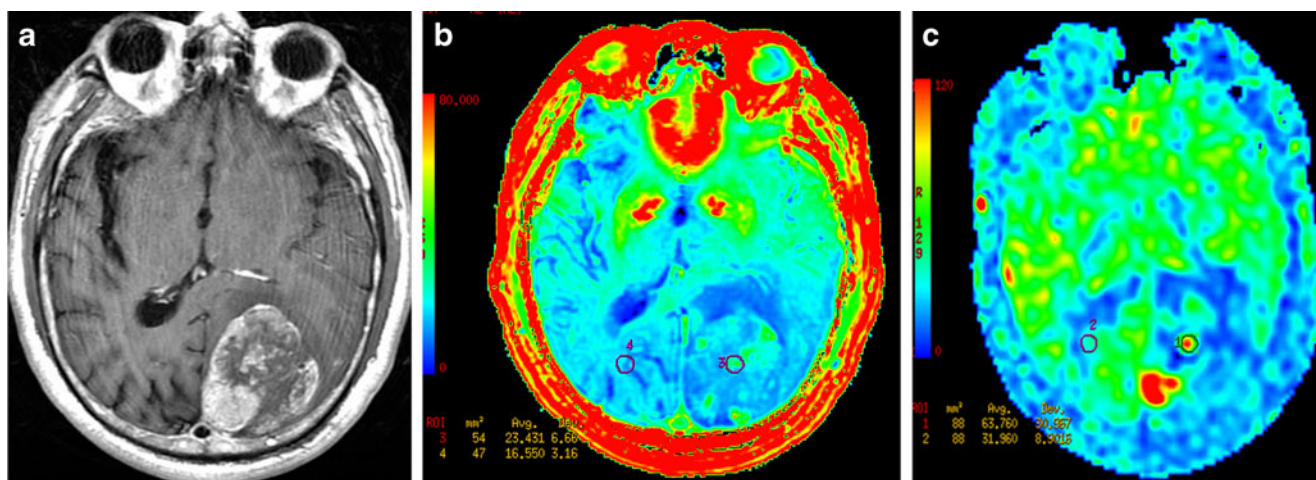


Fig. 4 A 70-year-old patient with a metastatic brain tumour underwent surgical resection, and the pathologic result was adenocarcinoma from lung cancer. **(a)** Contrast-enhanced T1-weighted image demonstrates a heterogeneous hyperintense mass in the left occipital lobe. **(b)** The

transverse R2* map shows the increased R2* values (23.43) in the tumour. **(c)** The ASL CBF map demonstrates marked perfusion in the central part of the mass

echoes was above 100. We considered that use of a 3.0-T MRI system resulted in higher SNRs of images. Therefore, our results were calculated using the 12 echoes.

Coregistration between R2* images and CE-T1WI images or DWI images was performed using geometric information stored in the respective data sets. On the R2* map, an ROI drawn in the tumour: (1) corresponded to the region with the maximum R2* value within the tumour; (2) corresponded to the enhanced region of the tumour on CE-T1WI images; (3) avoided the apparent haemorrhagic areas, which cause the high signal intensities on T1-weighted images or low signal intensities on T2-weighted images; (4) had a size of 30–150 mm².

R2* values of all tumours were measured three times by each neuroradiologist to obtain accurate results. Finally, we averaged R2* values of each ROI measured by the two neuroradiologists. In addition, ROIs were designated on rCBF

maps in the same regions within tumours as those on the R2* map, and rCBF values of tumours and the contralateral normal regions were recorded. Because the minimum ADCs correspond to the area of highest cellularity within tumours, we decided to measure minimum ADCs in the study.

We adopted rrCBF (the ratio of the rCBF value of the tumour to that of the contralateral normal region) in the study. R2*, rrCBF, and ADC values of all patients with tumours are listed in Table 1.

Statistical analysis

All data were statistically analysed using the Medcalc 12.0 and SPSS15.0 software packages. First, the interobserver agreement of R2* value measurements was tested by the Bland-Altman method [23]. Second, analysis of variance (ANOVA) was used to analyse R2* values and ADC values

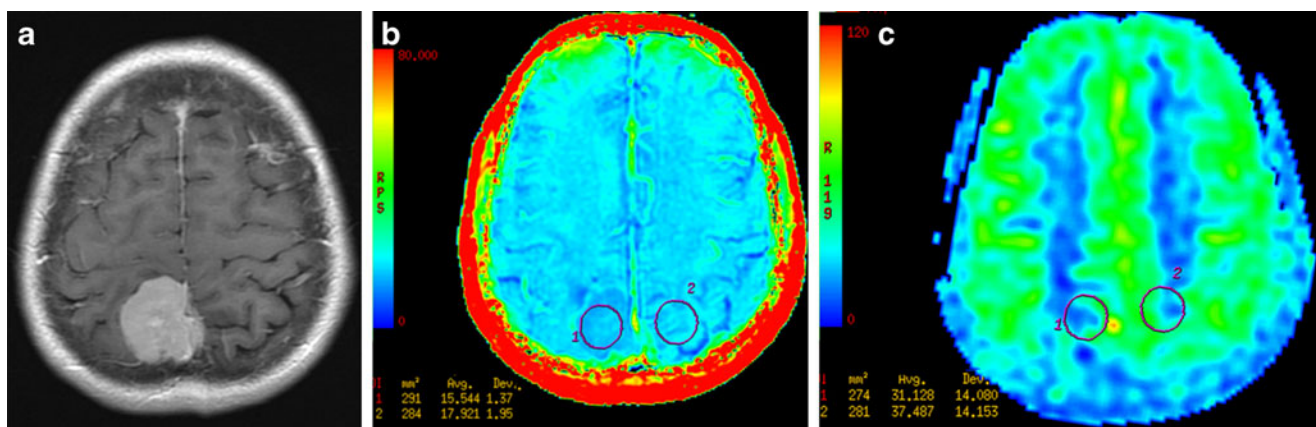


Fig. 5 A typical meningioma in a 48-year-old woman. **(a)** Transverse contrast-enhanced T1-weighted image shows intense enhancement of the tumour. **(b)** The R2* map shows there is a slightly lower R2* value in the

tumour (R2* value=15.54) than in the contralateral brain (R2* value=17.92). **(c)** The ASL CBF map shows the hypoperfusion in the tumour

among four grades of glioma. Then, the post-hoc all pairwise multiple comparisons (the Student-Newman-Keuls method) test was performed to test differences in $R2^*$ values among different grades of glioma. The Games-Howell post-hoc comparison test was used to analyse ADC values among four grades of glioma because variances were unequal.

Third, gliomas were divided into low grade (grades I and II) and high grade (grades III and IV). We used ANOVA to analyse $R2^*$ values among high-grade gliomas, low-grade gliomas, meningiomas, and brain metastasis. Then, the post-hoc all pairwise multiple comparisons (the Student-Newman-Keuls method) test was performed to test differences in $R2^*$ values among them. The independent t test was used to analyse $R2^*$, $rrCBF$, and ADC values of high- and low-grade gliomas.

Fourth, Spearman's correlation (a non-parametric test) coefficients were used to analyse the relationships among $R2^*$, $rrCBF$, and ADC values and the histopathological glioma grade. Pearson's correlation (a parametric test) was used to analyse the relationship between $R2^*$ and $rrCBF$ values in gliomas.

Fifth, $R2^*$, $rrCBF$, and ADC values of low- and high-grade gliomas were analysed with receiver-operator characteristic (ROCs) curves. Comparison of the area under the curve (AUC) was performed among three independent ROC curves. The ROC curve could be used to determine the optimal thresholds and diagnostic accuracy of $R2^*$ values for ascertaining high-grade gliomas. The ROC curve could also be used to calculate the sensitivity, specificity, PPV, and NPV associated with $R2^*$ values as a function of the threshold value used to identify high-grade gliomas. In fact, the four types of tumours can be classified into two grades, malignant (including high-grade gliomas and brain metastases) and benign (including low-grade gliomas and meningiomas), on the basis of their biological behaviours such as the recurrence and metastatic rates and the survival rate of patients. These two groups of $R2^*$ values underwent statistical analysis using ROC curves. The ROC curve was also used to analyse $R2^*$ values of brain metastasis and high-grade gliomas. P values of 0.05 were considered the criterion for statistical significance.

Results

There was good agreement in interobserver $R2^*$ value measurements because 96.88 % (62/64) of the points were inside the 95 % limits of agreement (−4.2 to 5.3) (Fig. 6).

The ANOVA test showed that $R2^*$ values were significantly different among the four grades of glioma ($F=36.071$, $P<0.001$). Then, the post hoc all pairwise multiple comparisons indicated that there were significant differences ($P<0.05$) in $R2^*$ values between grade I or grade II and grade III or grade IV gliomas. However, there were insignificant differences

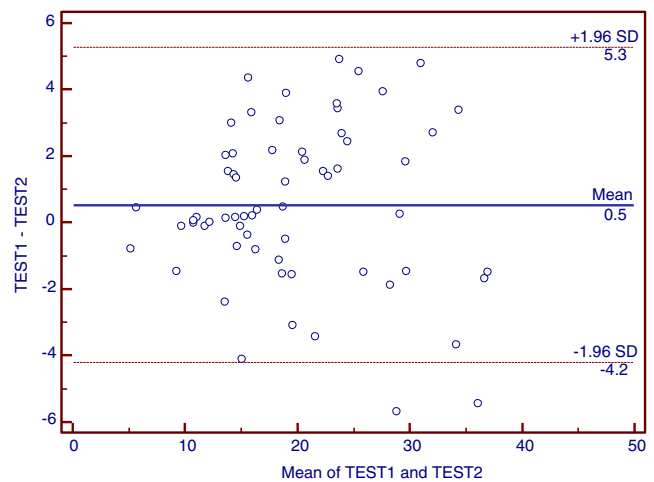


Fig. 6 Analysis of interobserver agreement of the $R2^*$ value measurements by the Bland-Altman method. There are 96.88 % (62/64) points inside the 95 % limits of agreement

between grade I and grade II ($P=0.724$) and between grade III and grade IV gliomas ($P=0.059$) (Table 2).

The ANOVA test indicated that $R2^*$ values were significantly different among high-grade gliomas, low-grade gliomas, meningiomas and brain metastasis ($F=38.733$, $P<0.001$). Post hoc comparisons indicated that there were significant differences in $R2^*$ values among high-grade gliomas, low-grade gliomas, meningiomas and brain metastasis. The mean $R2^*$ and $rrCBF$ values of four types of tumours are shown in Fig. 7.

$R2^*$ values showed a significant correlation with the histopathological grade of gliomas ($r=0.782$, $P<0.001$), which is shown in Fig. 8a. Additionally, there was no correlation between $R2^*$ values and $rrCBF$ values of gliomas (Pearson correlation coefficient=0.273, $P=0.08$).

$rrCBF$ values showed a significant correlation with the histopathological grade of gliomas ($r=0.643$, $P<0.05$). There was a significant difference in $rrCBF$ values between high- and low-grade gliomas ($t=4.61$, $P<0.001$).

The ANOVA test indicated that ADC values were insignificantly different among four grades of gliomas ($F=2.701$, $P=0.061$). Games-Howell post hoc comparisons indicated that there were insignificant differences among them (Table 2). A significant correlation existed between ADC values and the histopathological grade of gliomas ($r=-0.427$, $P=0.007$).

Table 2 The post hoc all pairwise multiple comparisons of $R2^*$ values and ADCs among four grades of glioma

Gliomas		$R2^*$ values	ADCs
I	II	0.724	0.928
	III	<0.05	0.395
	IV	<0.05	0.378
II	III	<0.05	0.147
	IV	<0.05	0.074
III	IV	0.059	1.000

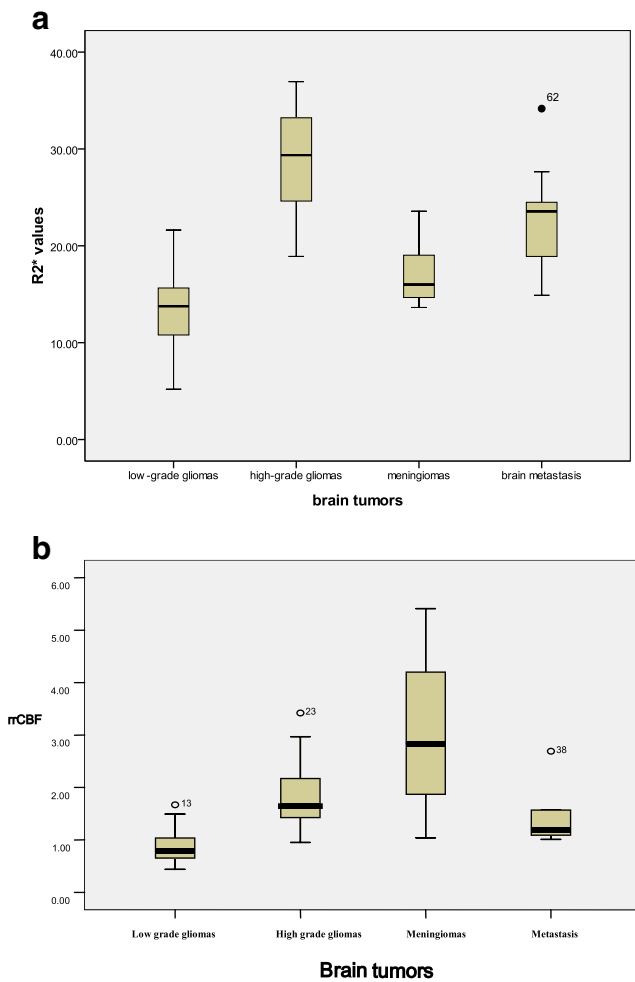


Fig. 7 R2* and rCBF values of four types of brain tumours. **(a)** The decreasing order of R2* values is high-grade gliomas, brain metastasis, meningiomas and low-grade gliomas. **(b)** The sequence rCBF values are meningiomas, high-grade gliomas, brain metastasis, and low-grade gliomas

(Fig. 8b). There was a significant difference in ADCs between high- and low-grade gliomas (Table 3).

In ROC curve analysis with histopathological correlation (Fig. 9), optimal sensitivity, specificity, PPV, and NPV in determining a high-grade glioma for differentiating low-grade gliomas by using an R2* value of 18.73 were 100 %, 95.5 %, 94.1 %, and 100 %, respectively. The areas under the ROC curve (AUC) for the R2* values was 0.994 (0.979–1.009). Comparison of the AUC showed there were significant differences in AUCs between R2* and ADC values ($z=3.714, P=0.0002$) and between rCBF and ADC values ($z=2.892, P=0.0038$), and an insignificant difference between R2* and rCBF values ($z=1.637, P=0.1016$) (Fig. 7).

In ROC curve analysis (Fig. 10), the R2* value (18.73) of malignant tumours provided a sensitivity of 85.7 %, specificity of 89.7 %, PPV of 83.87 %, and NPV of 90.9 % for differentiating benign tumours. The AUC for R2* values was 0.945

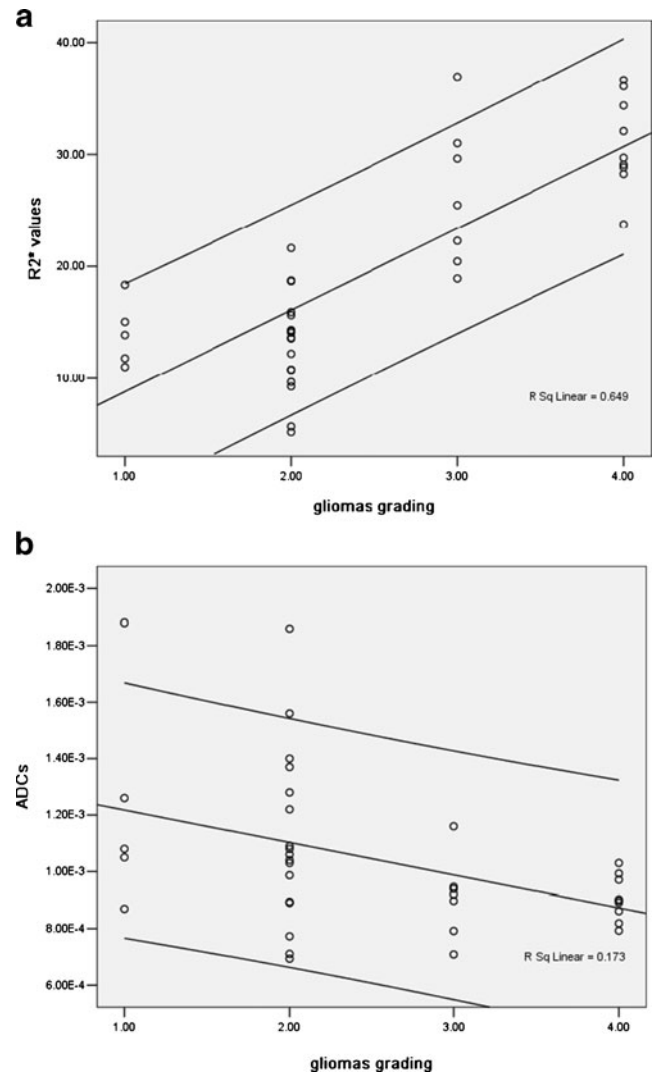


Fig. 8 Correlation analysis of R2* values or ADCs and the pathological grade of gliomas. **(a)** R2* values and the pathological grade of gliomas were strongly correlated, with Spearman’s coefficient $r=0.782 (P<0.05)$. There is a large overlap in R2* values between grade I and grade II as well as between grade III and grade IV. **(b)** A significant correlation ($r=-0.427; P=0.007$) exists between ADC values and the histopathological grade of gliomas. There are substantial overlaps in ADCs among four grades of glioma

(0.895–0.995). In ROC curve analysis (Fig. 11), optimal sensitivity, specificity, PPV, and NPV in differentiating high-grade gliomas from brain metastasis by using an R2* value of 27.65 were 68.7 %, 92.3 %, 91.7 %, and 70.6 %, respectively. The AUC for the R2* value was 0.815 (0.628–0.934).

Table 3 The independent *t* test of R2*, rCBF, and ADC values between high- and low-grade gliomas

	t	p
R2* values	9.940	<0.001
rCBF	4.333	<0.001
ADCs	3.149	0.004

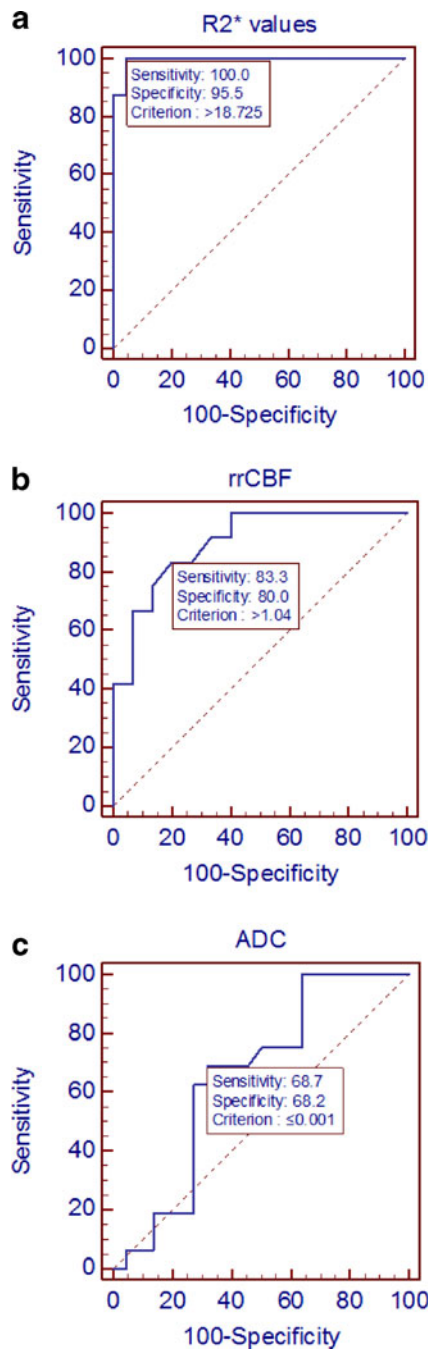


Fig. 9 **a, b, c** Receiver-operating characteristic (ROC) curve analysis of R2*, rrCBF, and ADC values for distinguishing low- from high-grade gliomas, respectively. ROC curve analyses of R2* values show larger AUCs than those of rrCBF and ADCs

Discussion

Significant differences existed in R2* values among four grades of glioma but not between grade I and grade II or between grade III and grade IV, which is consistent with the previous report on T2' values in tumours [22]. Further, R2* values correlated strongly with the grade of gliomas. Some studies have indicated there is a good correlation between

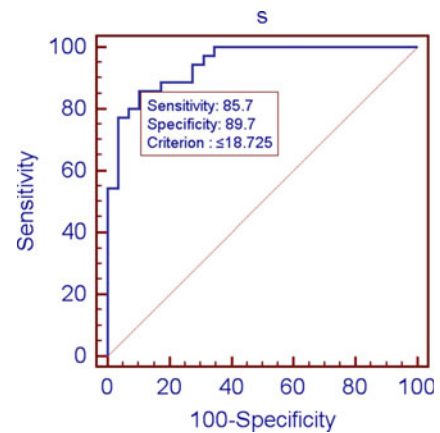


Fig. 10 ROC curve analysis for discriminating between malignant and benign tumours. The AUC for the R2* values is 0.945 (95 % CI, 0.895–0.995)

changes in R2* values and tumour pO₂ [24, 25]. Consequently, changes in the R2* value may reflect alterations in the deoxygenated haemoglobin concentration in tumour microvasculature [15, 16]. Our results may reflect that high-grade gliomas have higher deoxygenated haemoglobin concentrations than low-grade gliomas.

According to the ROC curve analysis, low-grade gliomas provided a sensitivity of 100 % and a specificity of 95.5 % for differentiating high-grade gliomas. This indicates that an R2* value of 18.73 can be recommended for discriminating high- from low-grade gliomas. Study results show that the R2* value is a useful adjunctive tool for assessing the grade of gliomas. There were significant differences in R2* values among high-grade gliomas, low-grade gliomas, meningiomas, and brain metastasis. However, there was marked overlap in R2* values between brain metastasis and high-grade gliomas. Furthermore, there were low sensitivity and NPV in the ROC curve analysis of brain metastasis and high-grade gliomas (Table 4). Therefore, it is difficult to differentiate high-grade glioma from brain metastasis with R2* values.

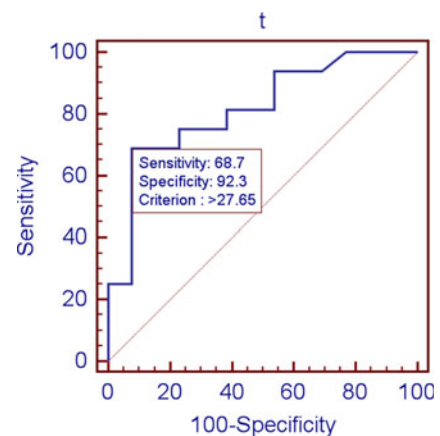


Fig. 11 ROC curve analysis of R2* values for distinguishing high-grade gliomas from metastasis. AUC for the R2* values is 0.815 (95 % CI, 0.628–0.934)

Table 4 Sensitivity, specificity, PPV, and NPV of R2* values for differentiating different types of brain tumours

Differential diagnosis	Sensitivity	Specificity	PPV	NPV
HGG vs. LGG	100 %	95 %	94.1 %	100 %
Malignant vs. benign	85.7 %	89.7 %	83.9 %	90.9 %
HGG vs. metastases	68.7 %	92.3 %	91.7 %	70.6 %

HGG indicates high-grade gliomas; LGG low-grade gliomas; PPV positive predictive value; NPV negative predictive value

There was a significant difference in R2* values between malignant and benign tumours and there were relatively high sensitivity, specificity, and PPV in the ROC curve (Table 4). This suggests that an R2* value of 18.73 can be recommended for distinguishing malignant from benign tumours. All of these results show that the R2* values differ among different tumours.

High-grade gliomas had significantly higher rCBF than low-grade gliomas (Table 3). This is in agreement with previous reports [26, 27]. However, the correlation coefficient between R2* values and grades of gliomas ($r=0.782$) was higher than that between rCBF values and grades of gliomas ($r=0.643$; $P<0.05$). This suggests that R2* values are better than rCBF for discriminating gliomas.

DWI, similar to rCBF, is believed to be a useful MRI technique for distinguishing low- from high-grade gliomas [9, 10]. Results show that there were insignificant differences among four grades of glioma and that there was a significant difference between high- and low-grade gliomas (Table 3). This is consistent with earlier reports [9, 10]. We consider that R2* values are far superior to minimum ADCs in distinguishing among different grades of glioma for the following reasons. First, there was substantial overlap in ADCs between different grades of glioma. Second, statistical analysis of AUCs showed that AUCs of R2* values were significantly higher than those of ADCs. Third, the correlation coefficient between R2* values and grades of gliomas ($r=0.782$) was higher than that between ADCs and grades of gliomas ($r=-0.427$).

We measured maximum R2* values in the study. Maximum R2* values have more instability and sensitivity than mean R2* values over a larger ROI. However, in the study, we set the ROI to more than 30 mm² to increase stability. Good agreement in interobserver R2* value measurements indicates there is better stability in the maximum R2* values.

On the R2* mapping sequence, MRI signal decay due to intravoxel dephasing depends on macroscopic B0 field variations, echo time, and pixel size [28, 29]. Macroscopic B0 field variations can induce additional intravoxel dephasing in the signal, which can overestimate R2* measurements [30]. Signal decay occurs more rapidly when there are longer echo times or greater pixel size in R2* mapping [31]. Automatic high-order B0 shimming is used to achieve high static

magnetic field homogeneity before R2* sequences. We used a 12-echo R2* sequence to obtain accurate R2* values in the study. However, longer echo times can cause faster signal decay, which can result in overestimation of R2* values. Therefore, we measured the image SNR before processing the R2* sequence. In the study methods, we planned to only use the images of the last four echoes if the SNR was above 100. In our study, the SNR of all images was above 100. Pixel size depends on FOV and matrix size. When the FOV is identical, greater pixel size needs a longer acquisition time. However, movement artefacts will increase when the acquisition time is longer. Movement artefacts can result in destructive interference of the extracted signals on R2* mapping. Therefore, in this study, we employed slightly smaller matrix size (192×160), which is greater than that in DWI (160×160).

There are some limitations in this study. First, as a preliminary study, the patient number was small. Second, the use of the T2* mapping sequence is limited in the tumour near air/tissue boundaries because of marked susceptibility artefacts. However, the advent of new techniques may solve this problem in the future [28].

In conclusion, as a preliminary observation, the study indicates that MR-based R2* values are a better tool than apparent diffusion coefficients or regional cerebral blood flow for determining the grade of gliomas and distinguishing benign from malignant tumours. With relatively short acquisition times and without the administration of contrast agent, the T2*-weighted sequence is a helpful adjunctive technique that can easily be incorporated as part of the routine MRI examination of intracranial tumours.

References

- Davis FG, Malmer BS, Aldape K et al (2008) Issues of diagnostic review in brain tumor studies: From the Brain Tumor Epidemiology Consortium. *Cancer Epidemiol Biomarkers Prev* 17:484–489
- Drevelgas A (2005) Extra-axial brain tumors. *Eur Radiol* 15:453–467
- Louis DN, Ohgaki H, Wiestler OD et al (2007) The 2007 WHO classification of tumours of the central nervous system. *Acta Neuropathol* 114:97–109
- Schiff D, Brown PD, Giannini C (2007) Outcome in adult low-grade glioma: the impact of prognostic factors and treatment. *Neurology* 69:1366–1373
- Butowski NA, Sneed PK, Chang SM (2006) Diagnosis and treatment of recurrent high-grade astrocytoma. *J Clin Oncol* 24:1273–1280
- Akiba T, Kunieda E, Kogawa A, Komatsu T, Tamai Y, Ohizumi Y (2012) Re-irradiation for metastatic brain tumors with whole-brain radiotherapy. *Jpn J Clin Oncol* 42:264–269
- Watts JM, Whitlow CT, Maldjian JA (2013) Clinical applications of arterial spin labeling. *NMR Biomed* 26:892–900
- Lanzman RS, Robson PM, Sun MR et al (2012) Arterial spin-labeling MR imaging of renal masses: correlation with histopathologic findings. *Radiology* 265:799–808

9. Murakami R, Hirai T, Sugahara T et al (2009) Grading astrocytic tumors by using apparent diffusion coefficient parameters: superiority of a one- versus two-parameter pilot method. *Radiology* 251:838–845
10. Higano S, Yun X, Kumabe T et al (2006) Malignant astrocytic tumors: clinical importance of apparent diffusion coefficient in prediction of grade and prognosis. *Radiology* 241:839–846
11. Noguchi T, Yoshiura T, Hiwatashi A et al (2008) Perfusion imaging of brain tumors using arterial spin-labeling: correlation with histopathologic vascular density. *AJNR* 29:688–693
12. Christen T, Bolar DS, Zaharchuk G (2013) Imaging brain oxygenation with MRI using blood oxygenation approaches: methods, validation, and clinical applications. *AJNR* 34:1113–1123
13. Bagley LJ, Grossman RI, Judy KD et al (1997) Gliomas: correlation of magnetic susceptibility artifact with histologic grade. *Radiology* 202:511–516
14. Barth M, Nöbauer-Huhmann IM, Reichenbach JR et al (2003) High-resolution three-dimensional contrast-enhanced blood oxygenation level-dependent magnetic resonance venography of brain tumors at 3 Tesla: first clinical experience and comparison with 1.5 Tesla. *Invest Radiol* 38:409–414
15. Punwani S, Ordidge RJ, Cooper CE, Amess P, Clemence M (1998) MRI measurements of cerebral deoxyhaemoglobin concentration [dHb]—correlation with near infrared spectroscopy (NIRS). *NMR Biomed* 11:281–289
16. Losert C, Peller M, Schneider P, Reiser M (2002) Oxygen-enhanced MRI of the brain. *Magn Reson Med* 48:271–277
17. Alonzi R, Padhani AR, Taylor NJ et al (2011) Antivascular effects of neoadjuvant androgen deprivation for prostate cancer: an in vivo human study using susceptibility and relaxivity dynamic MRI. *Int J Radiat Oncol Biol Phys* 80:721–727
18. McPhail LD, Robinson SP (2010) Intrinsic susceptibility MR imaging of chemically induced rat mammary tumors: relationship to histologic assessment of hypoxia and fibrosis. *Radiology* 254:110–118
19. Rodrigues LM, Howe FA, Griffiths JR, Robinson SP (2004) Tumor R2* is a prognostic indicator of acute radiotherapeutic response in rodent tumors. *J Magn Reson Imaging* 19:482–488
20. Müller A, Remmele S, Wenningmann I et al (2011) Analysing the response in R2* relaxation rate of intracranial tumours to hyperoxic and hypercapnic respiratory challenges: initial results. *Eur Radiol* 21:786–798
21. Kuperman VY, River JN (1995) Changes in T2* weighted images during hyperoxia differentiate tumors from normal tissue. *MRM* 33:318–325
22. Saitta L, Heese O, Förster AF et al (2011) Signal intensity in T2' magnetic resonance imaging is related to brain glioma grade. *Eur Radiol* 21:1068–1076
23. Bland JM, Altman DG (1986) Statistical methods for assessing agreement between two methods of clinical measurement. *Lancet* 1:307–310
24. Dunn JF, O'Hara JA, Zaim-Wadghiri Y et al (2002) Changes in oxygenation of intracranial tumors with carbogen: a BOLD MRI and EPR oximetry study. *J Magn Reson Imaging* 16:511–521
25. Zhao D, Jiang L, Hahn EW, Mason RP (2009) Comparison of 1H blood oxygen level-dependent (BOLD) and 19FMRItO investigate tumor oxygenation. *Magn Reson Med* 62:357–364
26. Warmuth C, Gunther M, Zimmer C (2003) Quantification of blood flow in brain tumors: comparison of arterial spin labeling and dynamic susceptibility weighted contrast-enhanced MR imaging. *Radiology* 228:523–532
27. Shin JH, Lee HK, Kwun BD et al (2002) Using relative cerebral blood flow and volume to evaluate the histopathologic grade of cerebral gliomas: preliminary results. *AJR* 179:783–789
28. Hernando D, Vigen KK, Shimakawa A et al (2012) R2* mapping in the presence of macroscopic B0 field variations. *Magn Reson Med* 68:830–840
29. De Guio F, Benoit-Cattin H, Davenel A (2008) Signal decay due to susceptibility-induced intravoxel dephasing on multiple air-filled cylinders: MRI simulations and experiments. *MAGMA* 21:261–271
30. Fernández-Seara MA, Wehrli FW (2000) Postprocessing technique to correct for background gradients in image-based R2* measurements. *Magn Reson Med* 44:358–366
31. Volz S, Hattingen E, Preibisch C et al (2009) Reduction of susceptibility-induced signal losses in multi-gradient-echo images: application to improved visualization of the subthalamic nucleus. *Neuroimage* 45:1135–1143